Atmos. Chem. Phys. Discuss., 15, 5203–5240, 2015
www.atmos-chem-phys-discuss.net/15/5203/2015/
doi:10.5194/acpd-15-5203-2015

Atmospheric Chemistry and Physics Discussions

Middle East versus Saharan dust extinction-to-backscatter ratios

A. Nisantzi[1], R. E. Mamouri[1], A. Ansmann[2], G. L. Schuster[3], and D. G. Hadjimitsis[1]

[1]Cyprus University of Technology, Dep. of Civil Engineering and Geomatics, Limassol, Cyprus
[2]Leibniz Institute for Tropospheric Research, Leipzig, Germany
[3]NASA Langley Research Center, Hampton, Virgina, USA

Received: 31 January 2015 – Accepted: 4 February 2015 – Published: 24 February 2015

Correspondence to: A. Nisantzi (argyro.nisantzi@cut.ac.cy)

Published by Copernicus Publications on behalf of the European Geosciences Union.

Abstract

Four years (2010–2013) of observations with polarization lidar and sun/sky photometer at the combined European Aerosol Research Lidar Network (EARLINET) and Aerosol Robotic Network (AERONET) site of Limassol (34.7° N, 33° E), Cyprus, were used to compare extinction-to-backscatter ratios (lidar ratios) for desert dust from Middle East deserts and the Sahara. The complex data analysis scheme is presented. The quality of the retrieval is checked within a case study by comparing the results with respective Raman lidar solutions for particle backscatter, extinction, and lidar ratio. The applied combined lidar/photometer retrievals corroborate recent findings regarding the difference between Middle East and Saharan desert dust lidar ratios. We found values from 44–65 sr with a mean value of 52.7 sr for Saharan dust and from 35–46 sr with a mean value of 41.1 sr for Middle East dust. The presented data analysis, however, also demonstrates the difficulties in identifying the optical properties of dust even during outbreak situations in the presence of complex aerosol mixtures of desert dust, marine particles, fire smoke, and anthropogenic haze.

1 Introduction

The particle extinction-to-backscatter ratio or lidar ratio S is an important quantity in the description of atmospheric aerosols with lidar (Müller et al., 2007; Burton et al., 2012; Groß et al., 2013) and a key input parameter in the retrieval of vertical profiles of the particle extinction coefficient from measurements with elastic backscatter lidars (Fernald, 1984; Ansmann, 2006) such as the spaceborne Cloud Aerosol Lidar with Orthogonal Polarization (CALIOP) (Omar et al., 2009). Profiles of the particle extinction coefficient throughout the troposphere and stratosphere belong to the basic input data sets in atmospheric modelling of the direct aerosol effect on climate. Dust-related extinction coefficient profiles are also used to estimate ice nuclei concentrations up to cirrus level (Mamouri and Ansmann, 2014b). Present and upcoming spaceborne lidar

ACPD
15, 5203–5240, 2015

activities (Winker et al., 2009; Stoffelen et al., 2005; Ansmann et al., 2007; Illingworth et al., 2015) need lidar-ratio information for all relevant aerosol types such as urban haze, biomass burning smoke, desert dust and marine particles in key areas of climate relevance for a consistent interpretation of the space-lidar-derived aerosol and cloud products.

Because desert dust is one of the major atmospheric aerosol components and the Sahara and the deserts in the Middle East (Syria, Jordan, Israel, Iraq, Arabian peninsula) are among the major dust sources of the world, the investigation and quantification of the optical properties including the lidar ratio of Saharan and Middle East dust is an important contribution to atmospheric and climate research. Recent Aerosol Robotic Network (AERONET) photometer-based studies of Schuster et al. (2012) and combined observations with polarization lidar and sun/sky photometer by Mamouri et al. (2013) suggest that lidar ratios of Middle East dust are significantly lower (35–45 sr) than the ones for Saharan dust (45–60 sr). The reason seems to be that the illite concentration in dust particles decreases from values around 80 % in western Saharan regions to less than 5 % in the dust particles in eastern Saharan and Middle East desert regions (Schuster et al., 2012). As a consequence the real part of the refractive index decreases from 1.55 for Arabian dust to 1.45 for western Saharan dust for the 500–550 nm wavelength range and the lidar ratio drops from values around 60 sr for western Saharan dust to values around or below 40 sr for Middle East dust. However, more studies are needed to corroborate these findings. Because photometers do not provide direct observations of 180° scattering, the lidar ratio cannot be measured and is obtained from modeling. A spheroidal particle shape model is used together with the observed spectral aerosol optical thickness (AOT) and sky radiance measurements to simulate the particle backscatter coefficient and the lidar ratio (Dubovik et al., 2006). The particle shape model assumes that the irregularly shaped dust particles are ideal spheroids. Because column-integrated particle information is measured when using photometers, lidar ratios for lofted dust layers above a polluted boundary layer (PBL) cannot be derived accurately.

ACPD
15, 5203–5240, 2015

The assumption of a spheroidal shape of the dust particles may cause uncertainties in the column dust lidar ratios of the order of 10 % or even more (Müller et al., 2010; Gasteiger et al., 2011; Wagner et al., 2013). However, Schuster et al. (2012) emphasized the strong influence of the real part of the refractive index on the particle optical properties. The real part dictates the scattering efficiency and has a strong impact on the computation of both, the AOT as well as the backscatter coefficient. Any pollution contribution (anthropogenic fine-mode haze) to the column aerosol observation was found to decrease the real part and to increase the column lidar ratio. Schuster et al. (2012) thus contrasted polluted dust for which the fine-mode volume fraction FVF is > 0.05 and pure dust scenarios with FVF < 0.05. All our observation discussed below are polluted dust cases.

We present, for the first time, a long-term lidar study on the lidar ratio of Middle East desert dust and compare the results with findings for Saharan dust outbreaks. The Limassol lidar station at the island of Cyprus in the eastern Mediterranean Sea is unique because it is the only site of the European Aerosol Research Lidar Network (EARLINET) which is influenced by a statistically significant number (5–7) of Middle East dust outbreaks each year as well as by numerous Saharan dust outbreaks ($> 10\,\mathrm{year}^{-1}$). A new polarization-lidar-based approach, introduced by Mamouri et al. (2013), is applied to extract the dust–related lidar ratio information from the total aerosol backscatter and extinction properties observed with the lidar as a function of height. In this study we considered 17 major dust outbreaks from the Middle East and 32 dust outbreaks from North Africa. Simultaneous EARLINET lidar and AERONET photometer observations were conducted at Limassol almost daily over the four-year period from May 2010 to December 2013.

There are already a lot of studies on Saharan dust lidar ratios mostly based on Raman lidar observations (Mattis et al., 2002; Amiridis et al., 2005; Mona et al., 2006; Papayannis et al., 2008; Esselborn et al., 2009; Tesche et al., 2009b, 2011; Groß et al., 2011; Preißler et al., 2013). For heavy dust loads the lidar ratio was typically in the range of 45–60 sr for western Saharan dust sources. Most lidars did not have a po-

ACPD
15, 5203–5240, 2015

larization sensitive channel for aerosol type separation so that it remains unknown to what extent the retrieval of dust optical properties is biased by the presence of non-dust particles. Respective efforts regarding Middle East dust are not available. A first lidar-based study of a strong Middle East desert dust outbreak was presented by Mamouri et al. (2013). Lidar ratios ranging from 34–39 sr were found. Here we extend this study and present a four-year statistics.

One of our goals is also to demonstrate how crucial the retrieval of pure Middle East desert dust lidar ratios is. As already observed during the United Arab Emirates Unified Aerosol Experiment (UAE^2) campaign (Reid et al., 2008), the Southwest Asian region is one of the most difficult environments of the world regarding characterizing, modeling and monitoring of the atmospheric state. Frequent dust storms, high pollution levels, and complex air flow pattern dominate the region. This is reflected in our observations, too.

In Sect. 2, the lidar and photometer instruments are briefly described. Section 3 presents the method applied to derive dust-related lidar ratios from elastic-backscatter signal profiles. The potential of the method is then discussed in Sect. 4 for the case of a major Saharan dust storm. Directly measured dust lidar-ratios, obtained by using the nitrogen Raman lidar signals in combination with the 532 nm elastic backscatter signals of the Limassol lidar during nighttime, are compared with respective dust lidar-ratio solutions obtained by means of our elastic-backscatter lidar approach (outlined in Sect. 3). The elastic-backscatter lidar approach is required because the majority of our lidar observations were performed at daytime simultaneously with the AERONET observations. The main findings of the study are given in Sect. 4. Summarizing and concluding remarks are presented in Sect. 5.

2 Instrumentation

The remote sensing station of the Cyprus University of Technology (CUT) at Limassol (34.7° N, 33° E, 50 m a.s.l.) is equipped with an EARLINET lidar (Mamouri

ACPD
15, 5203–5240, 2015

et al., 2013) and AERONET sun/sky photometer (CUT–TEPAK site, Limassol, Cyprus, http://aeronet.gsfc.nasa.gov) (Holben et al., 1998) and is located about 150 km south of Turkey and 250 km west of Syria.

The lidar transmits linearly polarized laser pulses at 532 nm and detects the parallel- and cross-polarized signal components. Further measurement channels collect lidar return signals at 607 nm (nitrogen Raman channel) and 1064 nm (elastic backscatter). The full overlap of the laser beam with the receiver field of view of the 20 cm Cassegrain telescope is obtained at heights around 300 m a.s.l. and therefore in most cases within the shallow planetary boundary layer (PBL) reaching up to 350–500 m height. An extended description of the instruments, the methods applied to analyze the data, the products, and retrieval uncertainties can be found in Mamouri et al. (2013) and Mamouri and Ansmann (2014a). In this paper, we will make use of the determined particle backscatter coefficient and the particle depolarization ratio at 532 nm.

The CUT AERONET photometer provides AOT measurements at eight wavelengths from 339 to 1638 nm. It also provides retrievals of particle size distributions, complex refractive index, and the number percentage of spherical particles (Dubovik and King, 2000). This is sufficient information to compute the column lidar ratio S_A (Schuster et al., 2012). From the particle size distribution the fine-mode volume fraction FVF is obtained. We further use the Ångström exponent AE (Ångström, 1964), determined from the spectral AOT distribution, and the fine mode fraction FMF (fraction of fine–mode AOT to total AOT) (O'Neill et al., 2003).

Our study includes a careful investigation of the air mass origin and long-range aerosol transport by means of backward trajectory analysis. The HYSPLIT (HYbrid Single-Particle Lagrangian Integrated Trajectory) model was used for this purpose. Access is provided via the NOAA ARL READY Website (http://www.arl.noaa.gov/HYSPLIT.php). HYSPLIT is described in detail by Draxler and Hess (1997, 1998), and Draxler (1999).

ACPD
15, 5203–5240, 2015

3 Data analysis procedure

The data analysis is based on simultaneous observations with polarization lidar and sun/sky photometer (daytime measurements) and follows the procedure outlined in Mamouri et al. (2013). For the correction of Rayleigh backscattering and extinction contributions to the observed signals we calculated the air molecule optical properties by assuming standard atmospheric conditions adjusted to actual surface conditions regarding temperature and pressure. The results in terms of particle backscatter coefficients differ by no more than a few percent (typically by 1 %) from calculation with temperature and pressure profiles taken from numerical weather prediction model outputs.

The following data analysis comprises ten steps. The products include the profiles of the particle backscatter coefficient separately for dust and non-dust aerosol components, the free tropospheric (FT) column dust and non-dust lidar ratios, and dust and non-dust-related particle optical depths of the lofted outbreak plumes. These ten steps are as follows:

1. We computed the profile of the particle backscatter coefficient after Mamouri et al. (2013) with the 500 nm AOT from the AERONET observations as a constraint. The conventional two-layer Fernald data analysis (Fernald, 1984; Ansmann, 2006; Mamouri et al., 2013) is applied. Layer 1 is the PBL reaching up to 350–500 m height. Layer 2 extends from the top of the PBL to the top of the lofted FT aerosol layer. By assuming a lidar ratio for the PBL of S_{PBL} = 25–35 sr, we obtain the particle lidar ratio S_T for the entire tropospheric column and S_{FT} for the free tropospheric column. The PBL over the coastal city contains a mixture of marine particles (lidar ratio of about 20 sr) and urban haze (lidar ratio of about 50 sr). The PBL AOT contribution is usually around 0.03. S_{PBL} values around 30 sr are typical for aerosol mixtures of anthropogenic haze and marine particles (Franke et al., 2001).

ACPD
15, 5203–5240, 2015

2. The particle linear depolarization ratio is calculated from the volume linear depolarization ratio by means of the particle backscatter coefficient profile (Freudenthaler et al., 2009; Tesche et al., 2009b).

3. HYSPLIT backward trajectory analysis together with the profiles of the particle depolarization ratio is used to identify cases with long-range transport of desert dust from the Middle East deserts or from northern Africa (Sahara region). 20–30 Middle East dust outbreaks of different strength crossed Cyprus during the four years under study. More than 50 cases of Saharan dust long-range transport were identified.

4. From the total set of dust outbreaks we considered only cases for further analysis (in Sect. 4) for which the particle linear depolarization ratio exceeded 0.15 in the free troposphere and this for a height range of at least 500 m. In this way, we obtained 17 Middle East dust cases and 32 Saharan dust cases for our dust lidar-ratio investigations.

5. In the next step, we calculated the geometrical properties of the remaining dust-containing layers (bottom and top heights). The height range for which the particle linear depolarization ratio is > 0.15 in the free troposphere represents the FT dust layer. Figure 1 shows bottom and top heights of all considered dust layers. The base of the FT dust layers frequently coincided with the top of the PBL. The depolarization ratio was often still high in the PBL. The top of the dust layers often reached to heights of 4–8 km a.s.l. This is in agreement with the spaceborne CALIOP lidar study presented by Liu et al. (2008).

6. For each layer, the layer-mean linear particle depolarization ratio and the corresponding SD, indicating the variability of the values within the layer, was computed. Figure 2 provides an overview of the obtained layer-mean particle linear depolarization ratios. In most cases, the mean depolarization ratio was in the

ACPD
15, 5203–5240, 2015

range from 0.17 to 0.28, and indicate aerosol mixtures with dust contributions to particle backscattering of 50–90 % according to Fig. 1 of Tesche et al. (2011).

7. By using the height profiles of the particle depolarization ratio and the particle backscatter coefficient we determine the dust and non-dust backscatter coefficient profiles (Tesche et al., 2009a) and, based on these profiles, we calculated the FT column backscatter values (Mamouri et al., 2013). In this approach, we assumed a particle linear depolarization ratio of 0.05 for non–dust particles and 0.31 for dust particles so that depolarization ratios < 0.05 and > 0.31 indicate a pure non-dust aerosol and a pure dust aerosol, respectively. Mixtures are indicated by depolarization ratios from > 0.05 to < 0.31.

8. In the retrieval of the FT dust lidar ratio $S_{FT,d}$ (in the next step 9), we need to assume a FT column lidar-ratio $S_{FT,s}$ for (spherical) non-dust particles. For this, we carefully inspected the backward trajectories. If the air masses crossed maritime areas only before arriving at Limassol, we selected $S_{FT,s}$ from 25–30 sr. This is for example the case when dust layers are advected from the Sahara on the most direct way. If the dust-laden air masses crossed industrialized and urbanized areas then we selected 50–55 sr for $S_{FT,s}$. If satellite imagery (Nisantzi et al., 2014) indicated that the air masses crossed even regions with biomass burning, we selected $S_{FT,s}$ of 65–70 sr. This step of the retrieval introduces a large uncertainty. It was found that the impact of the $S_{FT,s}$ assumption is low for FT dust backscatter fractions D_β of 0.75 and higher, and high for dust backscatter fractions around 0.5, which was frequently the case. The FT column dust backscatter fraction D_β is defined as the ratio of column-integrated dust backscatter coefficient to column-integrated total (dust and non-dust) particle backscatter coefficient for the free troposphere.

ACPD
15, 5203–5240, 2015

9. By using the selected $S_{FT,s}$ value, we estimated finally $S_{FT,d}$, after Eq. (4) in Mamouri et al. (2013). Rearrangement of this equation yields

$$S_{FT,d} = \frac{S_{FT} - (1 - D_\beta) S_{FT,s}}{D_\beta} \quad (1)$$

with the FT dust backscatter fraction D_β.

10. Finally we compute (a) the FT aerosol particle optical thickness AOT_{FT} from the particle backscatter coefficient profile and the column FT lidar ratio S_{FT}, (b) the FT dust and non-dust particle optical thicknesses $AOT_{FT,d}$ and $AOT_{FT,s}$ from the FT dust and non-dust backscatter coefficient profiles and the respective column lidar ratios $S_{FT,d}$ and $S_{FT,s}$, and (c) we estimated the dust fraction DF, i.e. the ratio $AOT_{FT,d}/AOT$ with the AOT as measured with AERONET photometer.

3.1 Retrieval uncertainties

As outlined in Mamouri et al. (2013), the uncertainty in $S_{FT,d}$ is mainly a function of the uncertainty in the assumed PBL lidar ratio S_{PBL} and the free tropospheric non-dust aerosol lidar ratio $S_{FT,s}$. By varying each of these two input lidar ratios by ±10 sr, the uncertainty range introduced by these assumptions can be realistically estimated. By considering a further uncertainty term resulting from a 10 % uncertainty in the separation of the dust and spherical particle components with the depolarization-ratio technique, the relative error of the dust lidar ratio $S_{FT,d}$ is about 20 % in cases of a strong dust outbreak with a dust fraction of > 0.75, and 25–50 % at aerosol conditions characterized by dust fraction of 0.3–0.6. In this error analysis, we ignore minor contributions by signal noise, uncertainties in the required Rayleigh extinction and backscatter calculations, and in the particle reference value, which may increase the overall relative uncertainty by further 5–10 %. We also ignore a minor impact of a few percent by the assumption of the backscatter profile slope in the lowermost 300 m (region of in-

ACPD
15, 5203–5240, 2015

complete laser-beam receiver-field-of-view overlap, see respective particle backscatter profile in several figures of Sect. 4).

However, if the assumption of the fine-mode aerosol lidar ratio $S_{FT,s}$ is wrong by 50–100 %, e.g., when erroneously a marine lidar ratio of 25 sr was assumed, but the true lidar ratio was 50 sr, the obtained uncertainty in the dust lidar ratio is of the order of 50–100 % as well. The influence of the $S_{FT,s}$ estimate is further discussed in the next section.

4 Results

4.1 Case study of 23 May 2013: Raman lidar observation

We checked the quality of the results obtained with the method described in Sect. 3 for cases where we could include the Raman signals in the aerosol analysis. The Raman lidar technique makes use of both, the elastic backscatter signals at 532 nm and the nitrogen Raman signals measured at 607 nm wavelength, and provides height profiles of the particle backscatter and extinction coefficients and thus a direct vertically resolved observation of the desert dust lidar ratio in pronounced dust layers (Mattis et al., 2002). In the following case study we compare the findings obtained with the Raman lidar method and with our approach (Sect. 3) which is based on elastic-backscatter signals, only.

Figure 3 shows the arrival of a thick Saharan dust plume over Limassol in the morning of 23 May 2013. According to the backward trajectories arriving above 2 km height at 19:00 UTC (see Fig. 4), the lofted Saharan dust layer between 2.5 and 5.5 km height originated from the central parts of the Sahara. Over about 4–5 days, dust could be collected by the air masses before traveling to Cyprus within 1–2 days. The layer below 2 km height contained a mixture of Saharan dust, European haze, and maritime particles according to the red backward trajectories for the arrival height of 1750 m.

ACPD
15, 5203–5240, 2015

An almost constant aerosol layering was observed above 2000 m from 17:30–20:50 UTC (see Fig. 3, second observational period after 17:30 UTC). We used this period for a detailed inspection of the optical properties of the Saharan dust plume by applying the Raman lidar method. Figure 5 shows the mean profiles of the 532 nm particle backscatter and extinction coefficients for the 17:47–20:50 UTC time period, and the respective height profile of the lidar ratio. The 532 nm dust optical depth was close to 0.38. As can be seen, in agreement with the backward trajectories, the lidar ratio shows typical Saharan dust values between 50–60 sr around the center of the dust layer at 3.5–4.0 km height. In the layer with aged European haze between 1.0 and 1.5 km height, the lidar ratio is close to 50 sr, and decreases to values below 30 sr at heights < 1.0 km height. Values of 25–35 sr are typical for a mixture of pollution and maritime particles (Franke et al., 2001).

In Fig. 6, the products obtained with our retrieval scheme (Sect. 3) are presented. Because after sunset no AERONET data are available, we used the lidar-derived AOT of 0.45 as a constraint in step 1 (see Sect. 3). The AOT was determined from the extinction profile in Fig. 6 (left panel) down to 1 km height and the backscatter profile below 1 km multiplied by a lidar ratio of 30 sr for the lowermost 1 km of the troposphere. As a result of step 1, we obtain the column lidar ratio of $S_{FT} = 57$ sr for the free troposphere and of $S_T = 55.8$ sr for the total tropospheric column. This value is close to the AERONET-derived total tropospheric lidar ratio of $S_{FT} = 58$ sr obtained from the afternoon photometer observations (13:00–14:00 UTC).

In step 2 of the data analysis, the particle linear depolarization ratio shown in Fig. 6 is computed. By means of the profiles of the particle backscatter coefficient and depolarization ratio the profile of the dust backscatter coefficient can then be calculated (step 7, red profile in Fig. 6) so that the column dust backscatter value for the free troposphere and the respective dust fraction D_β can be calculated (given as number in Fig. 6).

To obtain the dust-related lidar ratio $S_{FT,d}$ (step 8), we use Eq. (1). Disregarding the clear evidence that we observed a pronounced dust layer above 2 km on 23 May 2013,

ACPD
15, 5203–5240, 2015

we split the troposphere into the PBL (reaching up to 500 m) and the free troposphere (from 500–7000 m height). This was generally done for all cases of the four-year period discussed below. We assumed a PBL lidar ratio of $S_{PBL} = 30$ sr and a non-dust lidar ratio $S_{FT,s} = 50$ sr for the free troposphere accounting for the pollution particles mainly confined to the layer from 500–2000 m height.

The FT column dust backscatter value D_β of 0.834 in Fig. 6 indicates a dominating dust contribution to the measured optical effects. The FT column dust lidar ratio $S_{FT,d}$ was found to be close to 58 sr and thus close to the dust layer mean lidar ratio of 56 sr derived from the Raman lidar observations (see Fig. 5). The influence of uncertainties in the assumed PBL lidar ratio S_{PBL} on the retrieved dust lidar ratio $S_{FT,d}$ is low because the AOT of the PBL is less than 10 % of the total AOT. The uncertainty introduced by an error in the FT non-dust lidar ratio $S_{FT,s}$ of 10 sr results in an uncertainty of < 5 sr in the derived $S_{FT,d}$ value.

Next, we applied our data analysis procedure to the afternoon (12:59–13:59 UTC) observation on 23 May 2013. During daytime hours, AERONET AOT values are available (required in step 1 of our analysis). At this time of the day, the overall AOT at 500 nm was close to 0.32 and thus about 30 % lower than during the evening hours. As can be seen in Fig. 7, at the beginning of the dust outbreak period on 23 May 2013, the dust backscatter fraction was 0.672 in free troposphere (above 500 m height) and thus significantly lower than in the evening so that influence of the FT non-dust lidar ratio $S_{FT,s}$ was higher. Nevertheless, a good agreement between the dust lidar ratio $S_{FT,d}$ and the respective value obtained from the Raman lidar observations in the evening is found. Furthermore, the AERONET-derived lidar ratio $S_A = 58$ sr is in reasonable agreement with the lidar-derived lidar ratio $S_T = 51.5$ sr for the entire tropospheric column.

ACPD
15, 5203–5240, 2015

4.2 Case studies of 30 September 2010 (Saharan dust) and 17 May 2013 (Middle East dust)

All observational cases considered in our study were conducted at times from 07:00–14:00 UTC. For all cases sun photometer observations (AERONET or with hand-held Microtops photometer) are available. Figure 8 shows two further cases with pronounced dust layers above the PBL. According to the backward trajectories in Fig. 9 a Saharan dust layer and a Middle East desert dust plume were monitored. In both cases, the FT AOT of 0.16 and 0.87 strongly contributed to the total tropospheric AOT of 0.22 and 0.91, respectively. The dust backscatter fractions of 0.84 and 0.98 also indicate that dust dominated the optical properties in the free troposphere. The layer mean particle depolarization ratios were high with values of 0.26 (Saharan dust) and 0.30 (Middle East dust).

The comparably low AOT of 0.22 (Saharan dust case) was probably caused by the fact that only the lowest trajectory (red trajectory in the top panel of Fig. 9) was close to the ground over the desert so that considerable amounts of dust could enter the air mass over the Sahara at lower heights only. Because all Saharan trajectories indicate a direct air mass transport from the Sahara towards Cyprus (across the Mediterranean Sea) and therefore a very low influence of aged European on the aerosol mixture, we selected a non-dust lidar ratio for free tropospheric aerosols of $S_{FT,s} = 25$ sr which may indicate a slightly polluted marine aerosol. The resulting dust lidar ratio $S_{FT,d}$ was comparably low with a value of 47 sr. However, this value may be representative for the north-eastern Saharan region in agreement with the findings of Schuster et al. (2012) who noticed a steady decrease of the lidar ratio from values of 50–60 sr for western Saharan dust towards 40–45 sr for Middle East dust.

In contrast to the Saharan dust case, a large AOT of 0.91 was observed during a Middle East dust event on 17 May 2011. An almost pure dust plume reached from 500 m to 5 km height. According to the backward trajectories (see Fig. 9, lower panel) all air masses which crossed Cyprus between 2–5 km height were close to the ground

ACPD
15, 5203–5240, 2015

over the Middle East region. This explains the high dust load at all heights up to 5 km. Non-dust aerosol contributions were related to aged European haze, marine particles over the Mediterranean, and pollution over the western Asian states according to the backward trajectories. As a consequence, we selected a FT non-dust lidar ratio of $S_{FT,s}$ = 55 sr. However, at these dust-dominating conditions, this estimate (and the related uncertainties) has almost no influence on the result in terms of dust lidar ratio $S_{FT,d}$, which was 43 sr and thus close to the values found by Schuster et al. (2012) and Mamouri et al. (2013). Unfortunately we have no AERONET-derived lidar ratio for these two days because of problems with the photometer. Only hand-held Microtops sun photometer observations of the AOT could be performed on these days.

4.3 Statistics: Middle East vs. Saharan dust lidar ratios

Figures 10 and 11 provide an overview of all analyzed 17 major Middle East and 32 Saharan dust cases. The Middle East dust lidar ratios $S_{FT,d}$ are found in the range from 35–46 sr. The most accurate determination is given for dust backscatter fractions of $D_\beta > 0.8$ and layer mean particle depolarization ratios of > 0.25. At such conditions the uncertainty in the dust lidar ratio is of the order of 20 % or less. For the observed six cases with $D_\beta > 0.8$ (April 2011 to May 2012), $S_{FT,d}$ ranges from 42–46 sr in Fig. 10. For the less dust-dominated 11 cases with D_β from 0.15–0.7 and DF (dust AOT to total AOT) from 0.1–0.6 most dust lidar ratios were found between $S_{FT,d}$ = 35 and 40 sr. Here the uncertainty in the $S_{FT,d}$ values introduced by the non-dust lidar ratio assumptions is very high (of the order of 10–15 sr). The mean Middle East dust lidar ratio of all 17 cases is 41.1 ± 4.3 sr.

Figure 11 shows the retrieval results for the Saharan dust outbreaks. Here the dust lidar ratios $S_{FT,d}$ range from 44–65 sr. For the found six cases with $D_\beta > 0.8$ we obtain lidar ratios from 47–65 sr with four values in the range from 55–60 sr. We found 14 cases (out of the 32 Saharan dust cases) with layer mean particle depolarization ratios > 0.25. For these cases, the lidar ratios accumulate in the range from 50–55 sr. In contrast to the Middle East dust events, we assumed low FT non-dust lidar ratios $S_{FT,s}$

ACPD
15, 5203–5240, 2015

because the air masses have a comparably long distance across the Mediterranean Sea towards Cyprus and the pollution level over North Africa is lower than over the western Asian region. Most FT dust backscatter fractions D_β and Saharan DF values were in the range from 0.4–0.8 and 0.4–0.7, respectively, which clearly indicates that non-dust aerosol types always contributed to the observed particle backscatter and extinction properties. Thus, uncertainties in the $S_{FT,d}$ values of the order of 50 % introduced by the non-dust lidar ratio assumptions must be kept in consideration when discussing our findings. Nevertheless, the mean value of the 32 Saharan dust lidar ratios is 52.7 ± 6.1 sr. This lidar ratio is close to the value of 55 sr found by Tesche et al. (2009b) for pure Saharan dust cases.

Tables 1 and 2 provide additional insight into the aerosol mixing characteristics of the evaluated aerosol scenarios. Comparably high Ångström exponents were measured over Cyprus with the AERONET photometer during the dust events. These column observations always include the more polluted lowest parts of the atmosphere over the island. Pure dust extinction (and AOT) usually causes an Ånsgtröm exponents of 0.0–0.2. Also the fine mode fraction, FMF, is high compared to values of 0.2–0.3 for strong dust outbreaks (Mamouri and Ansmann, 2014a). Because the selection of the dust cases was guided by the particle depolarization ratio (> 0.15) in the same way and similar layer-mean depolarization ratios were found for both dust types, it is not surprising that all the properties listed in the two tables are similar.

Finally it is worth mentioning that the findings for the Middle East dust events (in Table 1) are in agreement with a study of Eck et al. (2008). During the UAE^2 campaign, performed in the United Arab Emirates and the adjacent Arabian Gulf region in August–September 2004, they found, on average, Ångström exponents of 0.5–0.77 (440–870 nm spectrum) for the 14 AERONET stations with slightly higher values for coastal and island sites compared to stations in the center of continental desert regions. Mean 500 nm FMF values ranged from 0.2–0.8. These values were mainly caused by strong fine-mode pollution particle sources from petroleum extraction and processing facilities. Only during rather strong dust events (over the desert stations)

ACPD
15, 5203–5240, 2015

the Ångström exponent dropped to typical dust values of 0.22–0.31 and the FMF were in the range from 0.24–0.29. According to Reid et al. (2008) and Eck et al. (2008) it was hard to observe pure dust optical properties, even in desert-dominated areas.

4.4 Comparison with AERONET observations of dust lidar ratios

Only a limited number of published lidar-ratio studies is available for comparison. As mentioned in the introduction, most lidar studies did not take the non-dust particle contribution to the observed mixed-aerosol lidar ratios into consideration. Cattrall et al. (2005) and Schuster et al. (2012) extensively discuss Saharan and Middle East dust lidar ratios based on AERONET observations. As also mentioned, these column-integrated measurements include the contribution of PBL aerosols (marine particles, local pollution, local road and soil dust) and are frequently affected by long-range transport of non-dust aerosol (fire smoke, lofted marine particles, aged anthropogenic pollution).

During events with a strong dust load with AOTs exceeding 0.4, Schuster et al. (2012) found mean values for the desert dust lidar ratio at 532 nm wavelength of 56.4 sr (over North African AERONET sites), 57.8 sr (Non-Sahel African stations), 55.1 sr (African Sahel sites), and 47.2 sr (AERONET stations in Middle East desert areas) for dust-dominated summer months from May to September in the years of 2006 to 2009. During very strong dust events (pure dust cases) with FVF < 0.05 and thus negligible impact of pollution particles on the computations the lidar ratios were on average about 10 % lower.

Cattrall et al. (2005) analyzed the main dust periods from 1994 to 2004 over eastern Asian, Middle East, and North African AERONET stations and found mean values of 39–41 sr for several Middle East sites and 35–38 sr for Saharan sites for the wavelength of 550 nm. Cattrall et al. (2005) used an older, less sophisticated AERONET inversion technique which may explain the differences with respect to the results of Schuster et al. (2012).

ACPD
15, 5203–5240, 2015

Figure 12 provides a comparison between lidar-based (S_T) and AERONET-based (S_A) retrieval results for the total tropospheric column. Six Middle East dust events and 14 Saharan dust cases are available for this comparison. Only this limited number of AERONET data could be analyzed. Most of the data are quality-assured AERONET data (level 2.0). However, the majority of AERONET observations were performed at AOTs clearly below 0.4 so that the uncertainty is high (Dubovik et al., 2000; Schuster et al., 2012). None of the shown cases passed the pure-dust criteria (FVF < 0.05). As mentioned in the introduction, the problem with fine-mode pollution is that these particles lower the overall refractive index. The fine mode is more optically efficient than the coarse mode, and increases the lidar ratio when compared to pure-dust scenarios. The impact of pollution aerosol is less dominant in the case of lidar retrievals (Fernald data analysis) at 532 nm wavelength. Coarse mode particles widely control the measured optical effects during dust outbreak situations. This is consistent with the results in Fig. 12. The tropospheric column lidar ratios retrieved from the AERONET observations are in most of the selected dust outbreak cases larger than the lidar-derived lidar ratios. We conclude from our analysis that AERONET-derived values overestimate the dust lidar ratio by about 20 %.

5 Conclusions

A study of dust particle lidar ratios for two major desert dust regions and sources for atmospheric dust has been presented. The particle lidar ratio is an important quantity in the description of atmospheric aerosols and aerosol mixtures in the framework of aerosol typing efforts. It is a key input parameter in the retrieval of height profiles of climate relevant particle extinction coefficient, derived from widely used elastic backscatter lidars including the spaceborne lidar CALIOP. Present and upcoming spaceborne lidar activities need lidar-ratio information for all relevant aerosol types for a consistent interpretation of the space-lidar-derived aerosol and cloud products around the globe.

ACPD
15, 5203–5240, 2015

We found a significant difference with mean values of 52.7 ± 6.1 and 41.1 ± 4.3 sr for Saharan and Middle East desert dust, respectively, which is in good agreement with literature values. A recently introduced polarization lidar technique (Mamouri et al., 2013) for the extraction of dust lidar ratio information from elastic-backscatter lidar observations was applied to the four-year Cyprus data set.

The study corroborates earlier findings that desert dust plumes contain a mixture of desert dust and a variety of other aerosol components (marine particles, fire smoke, anthropogenic haze). Lofted pure desert dust plumes are more the exception than the rule. From this point of view it is a rather difficult effort to select the optimum lidar ratio in the analysis of CALIOP observations over deserts and adjacent regions. The measurement of the particle depolarization ratio is demanding in order to be able to identify and quantify the dust contribution to the aerosol load and more generally for a high-quality aerosol typing.

Acknowledgements. The authors thank the CUT Remote Sensing Laboratory for their support. The work was co-funded by the European Regional Development Fund and the Republic of Cyprus through the Research Promotion Foundation (PENEK/0311/05). The research leading to these results has also received scientific support from the European Union Seventh Framework Programme (FP7/2011–2015) under grant agreement no. 262 254 (ACTRIS project). The authors gratefully acknowledge the NOAA Air Resources Laboratory (ARL) for the provision of the HYSPLIT transport and dispersion model as well for the provision of Global Data Assimilation System (GDAS) data used in this publication. We are also grateful to AERONET for high-quality sun/sky photometer measurements.

References

Amiridis, V., Balis, D. S., Kazadzis, S., Bais, A., Giannakaki, E., Papayannis, A., and Zerefos, C.: Four-year aerosol observations with a Raman lidar at Thessaloniki, Greece, in the framework of European Aerosol Research Lidar Network (EARLINET), J. Geophys. Res., 110, D21203, doi:10.1029/2005JD006190, 2005. 5206

ACPD
15, 5203–5240, 2015

Amiridis, V., Wandinger, U., Marinou, E., Giannakaki, E., Tsekeri, A., Basart, S., Kazadzis, S., Gkikas, A., Taylor, M., Baldasano, J., and Ansmann, A.: Optimizing CALIPSO Saharan dust retrievals, Atmos. Chem. Phys., 13, 12089–12106, doi:10.5194/acp-13-12089-2013, 2013.
Ångström, A.: The parameters of atmospheric turbidity, Tellus, 16, 64–75, 1964. 5208
Ansmann, A.: Ground-truth aerosol lidar observations: can the Klett solutions obtained from ground and space be equal for the same aerosol case?, Appl. Optics, 45, 3367–3371, 2006. 5204, 5209
Ansmann, A., Wandinger, U., Le Rille, O., Lajas, D., and Straume, A. G.: Particle backscatter and extinction profiling with the spaceborne high-spectral-resolution Doppler lidar ALADIN: methodology and simulations, Appl. Opt, 46, 6606–6626, 2007. 5205
Ansmann, A., Baars, H., Tesche, M., Müller, D., Althausen, D., Engelmann, R., Pauliquevis, T., and Artaxo, P.: Dust and smoke transport from Africa to South America: lidar profiling over Cape Verde and the Amazon rainforest, Geophys. Res. Lett., 36, L11802, doi:10.1029/2009GL037923, 2009.
Baars, H., Ansmann, A., Althausen, D., Engelmann, R., Artaxo, P., Pauliquevis, T., and Souza, R.: Further evidence for significant smoke transport from Africa to Amazonia, Geophys. Res. Lett., 38, L20802, doi:10.1029/2011GL049200, 2011.
Burton, S. P., Ferrare, R. A., Hostetler, C. A., Hair, J. W., Rogers, R. R., Obland, M. D., Butler, C. F., Cook, A. L., Harper, D. B., and Froyd, K. D.: Aerosol classification using airborne High Spectral Resolution Lidar measurements – methodology and examples, Atmos. Meas. Tech., 5, 73–98, doi:10.5194/amt-5-73-2012, 2012. 5204
Cattrall, C., Reagan, J., Thome, K., and Dubovik, O.: Variability of aerosol and spectral lidar and backscatter and extinction ratios of key aerosol types derived from selected Aerosol Robotic Network locations, J. Geophys. Res., 110, D10S11, doi:10.1029/2004JD005124, 2005. 5219
Draxler, R. R.: HYSPLIT4 User's Guide, NOAA Tech. Memo. ERL ARL-230, NOAA Air Resources Laboratory, Silver Spring, MD, 1999. 5208
Draxler, R. R. and Hess, G. D.: Description of the HYSPLIT 4 Modeling System, NOAA Tech. Memo. ERL ARL–224, NOAA Air Resources Laboratory, Silver Spring, MD, 1997. 5208
Draxler, R. R. and Hess, G. D.: An overview of the HYSPLIT 4 modeling system of trajectories, dispersion, and deposition, Aust. Meteorol. Mag., 47, 295–308, 1998. 5208
Dubovik, O. and King, M.: A flexible inversion algorithm for retrieval of aerosol optical properties from Sun and sky radiance measurements, J. Geophys. Res., 105, 20673–20696, doi:10.1029/2000JD900282, 2000. 5208

ACPD
15, 5203–5240, 2015

Dubovik, O., Smirnov, A., Holben, B. N., King, M. D., Kaufman, Y. J., Eck, T. F., and Slutsker, I.: Accuracy assessments of aerosol optical properties retrieved from Aerosol Robotic Network (AERONET) Sun and sky radiance measurements, J. Geophys. Res., 105, 9791–9806, doi:10.1029/2000JD900040, 2000. 5220

Dubovik, O., Sinyuk, A., Lapyonok, T., Holben, B. N., Mishchenko, M., Yang, P., Eck, T. F., Voltne, H., Munoz, O., Veihelmann, B., Van der Zande, W., J., Leon, J.-F., Sorokin, M., and Slutsker, I.: Application of spheroid models to account for aerosol particle nonsphericity in remote sensing of desert dust, J. Geophys. Res., 111, D11208, doi:10.1029/2005JD006619, 2006. 5205

Eck, T. F., Holben, B. N., Reid, J. S., Sinyuk, A., Dubovik, O., Smirnov, A., Giles, D., O'Neill, N. T., Tsay, S.-C., Ji, Q., Al Mandoos, A., Ramzan Khan, M., Reid, E. A., Schafer, J. S., Sorokine, M., Newcomb, W., and Slutsker, I.: Spatial and temporal variability of column-integrated aerosol optical properties in the southern Arabian Gulf and United Arab Emirates in summer, J. Geophys. Res., 113, D01204, doi:10.1029/2007JD008944, 2008. 5218, 5219

Esselborn, M., Wirth, M., Fix, A., Weinzierl, B., Rasp, K., Tesche, M., and Petzold, A.: Spatial distribution and optical properties of Saharan dust observed by airborne high spectral resolution lidar during SAMUM 2006, Tellus B, 61, 131–143, doi:10.1111/j.1600-0889.2008.00394.x, 2009. 5206

Fernald, F. G.: Analysis of atmospheric lidar observations: some comments, Appl. Optics, 23, 652–653, 1984. 5204, 5209

Franke, K., Ansmann, A., Müller, D., Althausen, D., Wagner, F., and Scheele, R.: One-year observations of particle lidar ratio over the tropical Indian Ocean with Raman lidar, Geophys. Res. Lett., 28, 4559–4562, doi:10.1029/2001GL013671, 2001. 5209, 5214

Freudenthaler, V., Esselborn, M., Wiegner, M., Heese, B., Tesche, M., Ansmann, A., Müller, D., Althausen, D., Wirth, M., Fix, A., Ehret, G., Knippertz, P., Toledano, C., Gasteiger, J., Garhammer, M., and Seefeldner, M.: Depolarization ratio profiling at several wavelengths in pure Saharan dust during SAMUM 2006, Tellus B, 61, 16579, doi:10.1111/j.1600-0889.2008.00396.x, 2009. 5210

Gasteiger, J., Wiegner, M., Groß, S., Freudenthaler, V., Toledano, C., Tesche, M., and Kandler, K.: Modelling lidar-relevant optical properties of complex mineral dust aerosols, Tellus B, 63, 725–741, doi:10.1111/j.1600-0889.2011.00559.x, 2011. 5206

Groß, S., Tesche, M., Freudenthaler, V., Toledano, C., Wiegner, M., Ansmann, A., Althausen, D., and Seefeldner, M.: Characterization of Saharan dust, marine aerosols and mixtures of

ACPD
15, 5203–5240, 2015

biomass-burning aerosols and dust by means of multi-wavelength depolarization and Raman lidar measurements during SAMUM 2, Tellus B, 63, 706724, doi:10.1111/j.1600-0889.2011.00556.x, 2011. 5206

Groß, S., Esselborn, M., Weinzierl, B., Wirth, M., Fix, A., and Petzold, A.: Aerosol classification by airborne high spectral resolution lidar observations, Atmos. Chem. Phys., 13, 2487–2505, doi:10.5194/acp-13-2487-2013, 2013. 5204

Holben, B. N., Eck, T. F., Slutsker, I., Tanré, D., Buis, J. P., Setzer, A., Vermote, E., Reagan, J. A., Kaufman, Y. J., Nakajima, T., Lavenu, F., Jankowiak, I., and Smirnov, A.: AERONET – a federated instrument network and data archive for aerosol characterization, Remote Sens. Environ., 66, 1–16, 1998. 5208

Illingworth, A. J., Barker, H. W., Beljaars, A., Ceccaldi, M., Chepfer, H., Clerbaux, N., Cole, J., Delanoe, J., Domenech, C., Donovan, D. P., Fukuda, S., Hirakata, M., Hogan, R. J., Huenerbein, A., Kollias, P., Kubota, T., Nakajima, T., Nakajima, T. Y., Nishizawa, T., Ohno, Y., Okamoto, H., Oki, R., Sato, K., Satoh, M., Shephard, M., Velazquez Blazquez, A., Wandinger, U., Wehr, T., and van Zadelhoff, G.-J.: The Earthcare Satellite: the next step forward in global measurements of clouds, aerosols, precipitation and radiation, B. Am. Meteorol. Soc., 96, doi:10.1175/BAMS-D-12-00227.1, in press, 2015. 5205

Liu, D., Wang, Z., Liu, Z., Winker, D., and Trepte, C.: A height resolved global view of dust aerosols from the first year CALIPSO lidar measurements, J. Geophys. Res., 113, D16214, doi:10.1029/2007JD009776, 2008. 5210

Mamouri, R. E. and Ansmann, A.: Fine and coarse dust separation with polarization lidar, Atmos. Meas. Tech., 7, 3717–3735, doi:10.5194/amt-7-3717-2014, 2014a. 5208, 5218

Mamouri, R. E. and Ansmann, A.: Dust-related ice nuclei profiles from polarization lidar: methodology and case studies, Atmos. Chem. Phys. Discuss., 14, 25747–25786, doi:10.5194/acpd-14-25747-2014, 2014b. 5204

Mamouri, R. E., Ansmann, A., Nisantzi, A., Kokkalis, P., Schwarz, A., and Hadjimitsis, D.: Low Arabian dust extinction-to-backscatter ratio, Geophys. Res. Lett., 40, 4762–4766, doi:10.1002/grl.50898, 2013. 5205, 5206, 5207, 5208, 5209, 5211, 5212, 5217, 5221

Mattis, I., Ansmann, A., Müller, D., Wandinger, U., and Althausen, D.: Dual-wavelength Raman lidar observations of the extinction-to-backscatter ratio of Saharan dust, Geophys. Res. Lett., 29, 1306, doi:10.1029/2002GL014721, 2002. 5206, 5213

ACPD
15, 5203–5240, 2015

Mona, L., Amodeo, A., Pandolfi, M., and Pappalardo, G.: Saharan dust intrusions in the Mediterranean area: three years of Raman lidar measurements, J. Geophys. Res., 111, D16203, doi:10.1029/2005JD006569, 2006. 5206
Müller, D., Ansmann, A., Mattis, I., Tesche, M., Wandinger, U., Althausen, D., and Pisani, G.: Aerosol-type-dependent lidar ratios observed with Raman lidar, J. Geophys. Res., 112, D16202, doi:10.1029/2006JD008292, 2007. 5204
Müller, D., Weinzierl, B., Petzold, A., Kandler, K., Ansmann, A., Müller, T., Tesche, M., Freudenthaler, V., Esselborn, M., Heese, B., Althausen, D., Schladitz, A., Otto, S., and Knippertz, P.: Mineral dust observed with AERONET Sun photometer, Raman lidar and in situ instruments during SAMUM 2006: shape-independent particle properties, J. Geophys. Res., 115, D11207, doi:10.1029/2009JD012523, 2010. 5206
Nisantzi, A., Mamouri, R. E., Ansmann, A., and Hadjimitsis, D.: Injection of mineral dust into the free troposphere during fire events observed with polarization lidar at Limassol, Cyprus, Atmos. Chem. Phys., 14, 12155–12165, doi:10.5194/acp-14-12155-2014, 2014. 5211
Omar, A. H., Winker, D. M., Kittaka, C., Vaughan, M. A., Liu, Z., Hu, Y., Trepte, C. R., Rogers, R. R., Ferrare, R. A., Lee, K.-P., Kuehn, R. E., and Hostetler, C. A.: The CALIPSO automated aerosol classification and lidar ratio selection algorithm, J. Atmos. Ocean. Tech., 26, 1994–2014, doi:10.1175/2009JTECHA1231.1, 2009. 5204
O'Neill, N. T., Eck, T. F., Smirnov, A., Holben, B. N., and Thulasiraman, S.: Spectral discrimination of coarse and fine mode optical depth, J. Geophys. Res., 108, 4559, doi:10.1029/2002JD002975, 2003. 5208
Papayannis, A., Amiridis, V., Mona, L., Tsaknakis, G., Balis, D., Bösenberg, J., Chaikovski, A., De Tomasi, F., Grigorov, I., Mattis, I., Mitev, V., Müller, D., Nickovic, S., Pérez, C., Pietruczuk, A., Pisani, G., Ravetta, F., Rizi, V., Sicard, M., Trickl, T., Wiegner, M., Gerding, M., Mamouri, R. E., D'Amico, G., and Pappalardo, G.: Systematic lidar observations of Saharan dust over Europe in the frame of EARLINET (2000–2002), J. Geophys. Res., 113, D10204, doi:10.1029/2007JD009028, 2008. 5206
Preißler, J., Wagner, F., Guerrero-Rascado, J. L., and Silva, A. M.: Two years of free-tropospheric aerosol layers observed over Portugal by lidar, J. Geophys. Res.-Atmos., 118, 3676–3686, doi:10.1002/jgrd.50350, 2013. 5206
Reid, J. S., Piketh, S. J., Walker, A. L., Burger, R. P., Ross, K. E., Westphal, D. L., Bruintjes, R. T., Holben, B. N., Hsu, C., Jensen, T. L., Kahn, R. A., Kuciauskas, A. P., Al Mandoo, A., Mangoosh, A., Miller, S. D., Porter, J. N., Reid, E. A., and Tsay, S.-C.: An overview of UAE2 flight

ACPD
15, 5203–5240, 2015

operations: observations of summertime atmospheric thermodynamic and aerosol profiles of the southern Arabian Gulf, J. Geophys. Res., 113, D14213, doi:10.1029/2007JD009435, 2008. 5207, 5219

Schuster, G. L., Vaughan, M., MacDonnell, D., Su, W., Winker, D., Dubovik, O., Lapyonok, T., and Trepte, C.: Comparison of CALIPSO aerosol optical depth retrievals to AERONET measurements, and a climatology for the lidar ratio of dust, Atmos. Chem. Phys., 12, 7431–7452, doi:10.5194/acp-12-7431-2012, 2012. 5205, 5206, 5208, 5216, 5217, 5219, 5220, 5234, 5240

Stoffelen, A., Pailleux, J., Källén, E., Vaughan, J. M., Isaksen, L., Flamant, P., Wergen, W., Andersson, E., Schyberg, H., Culoma, A., Meynart, R., Endemann, M., and Ingmann, P.: The Atmospheric Dynamics Mission for global wind field measurements, B. Am. Meteorol. Soc., 86, 73–87, 2005. 5205

Tesche, M., Ansmann, A., Müller, D., Althausen, D., Engelmann, R., Freudenthaler, V., and Groß, S.: Vertically resolved separation of dust and smoke over Cape Verde using multiwavelength Raman and polarization lidars during Saharan Mineral Dust Experiment 2008, J. Geophys. Res., 114, D13202, doi:10.1029/2009JD011862, 2009a. 5211

Tesche, M., Ansmann, A., Müller, D., Althausen, D., Mattis, I., Heese, B., Freudenthaler, V., Wiegner, M., Eseelborn, M., Pisani, G., and Knippertz, P.: Vertical profiling of Saharan dust with Raman lidars and airborne HSRL in southern Morocco during SAMUM, Tellus B, 61, 144–164, doi:10.1111/j.1600-0889.2008.00390.x, 2009b. 5206, 5210, 5218

Tesche, M., Groß, S., Ansmann, A., Müller, D., Althausen, D., Freudenthaler, V., and Esselborn, M.: Profiling of Saharan dust and biomass-burning smoke with multiwavelength polarization Raman lidar at Cape Verde, Tellus B, 63, 649–676, doi:10.1111/j.1600-0889.2011.00548.x, 2011. 5206, 5211

Wagner, J., Ansmann, A., Wandinger, U., Seifert, P., Schwarz, A., Tesche, M., Chaikovsky, A., and Dubovik, O.: Evaluation of the Lidar/Radiometer Inversion Code (LIRIC) to determine microphysical properties of volcanic and desert dust, Atmos. Meas. Tech., 6, 1707–1724, doi:10.5194/amt-6-1707-2013, 2013. 5206

Winker, D. M., Vaughan, M. A., Omar, A., Hu, Y., Powell, K. A., Liu, Z., Hunt, W. H., and Young, S. A.: Overview of the CALIPSO mission and CALIOP data processing algorithms, J. Atmos. Ocean. Tech., 26, 2310–2323, doi:10.1175/2009JTECHA1281.1, 2009. 5205

ACPD
15, 5203–5240, 2015

Table 1. Middle East desert dust cases (17 cases, 2010–2013): AERONET Ångström exponent (440–870 nm) and fine-mode fraction (ratio of 500 nm fine-mode AOT to AOT) for the tropospheric vertical column (T), and lidar-derived 532 nm dust AOT for the free troposphere, dust fraction in the free troposphere (ratio of 532 nm FT dust AOT to FT AOT) and FT mean particle linear depolarization ratio (532 nm). Mean and SD of all cases are given together with the range of observed values (from minimum to maximum value).

Parameter	Mean	SD	Min	Max
Ångström exponent (T)	0.755	0.380	0.060	1.246
Fine-mode fraction (T)	0.499	0.109	0.376	0.683
Dust AOT (FT)	0.218	0.197	0.042	0.848
Dust AOT fraction (FT)	0.619	0.241	0.179	0.975
Depolarization ratio	0.237	0.049	0.174	0.384

ACPD
15, 5203–5240, 2015

Table 2. Same as Table 1, but for the 32 selected major Saharan dust outbreaks.

Parameter	Mean	SD	Min	Max
Ångström exponent (T)	0.735	0.464	0.044	1.626
Fine-mode fraction (T)	0.380	0.154	0.176	0.619
Dust AOT (FT)	0.177	0.204	0.050	1.146
Dust fraction (FT)	0.662	0.175	0.354	0.990
Depolarization ratio	0.242	0.038	0.186	0.324

ACPD
15, 5203–5240, 2015

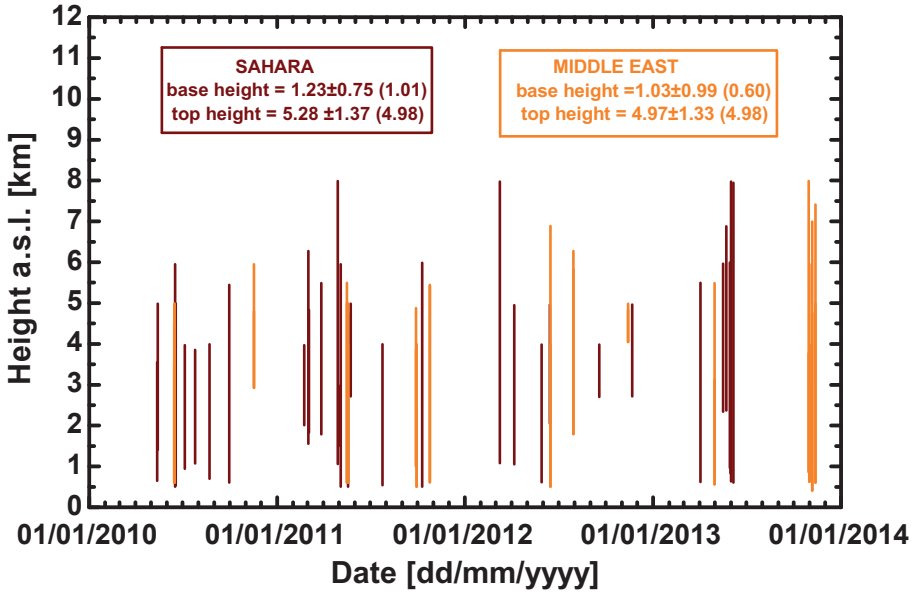

Figure 1. Lofted free–tropospheric desert dust layers (shown as vertical lines from bottom to top) observed between April 2010 and December 2013. The brown and orange vertical lines indicate 32 Saharan dust and 17 Middle East dust cases. The average bottom and top heights (plus the SD) of all detected dust layers are given as numbers. Median values are given in parentheses.

ACPD
15, 5203–5240, 2015

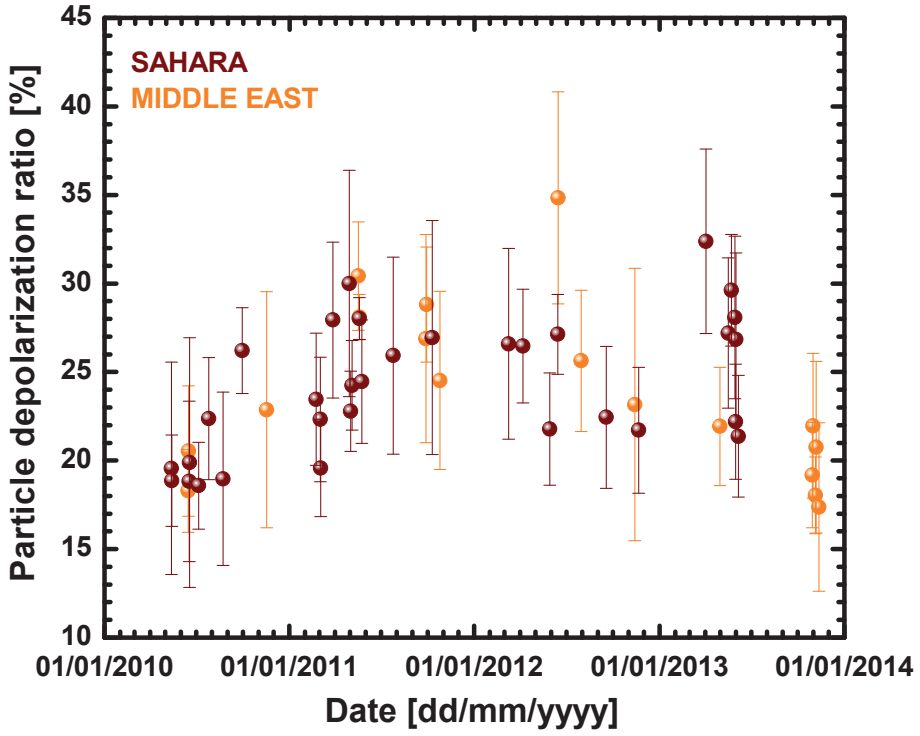

Figure 2. Free-tropospheric dust layer mean particle linear depolarization ratio of all 32 Saharan dust (brown circles) and 17 Middle East dust cases (orange circles). The shown SDs (vertical bars) indicate the atmospheric variability in terms of the FT depolarization ratio.

ACPD
15, 5203–5240, 2015

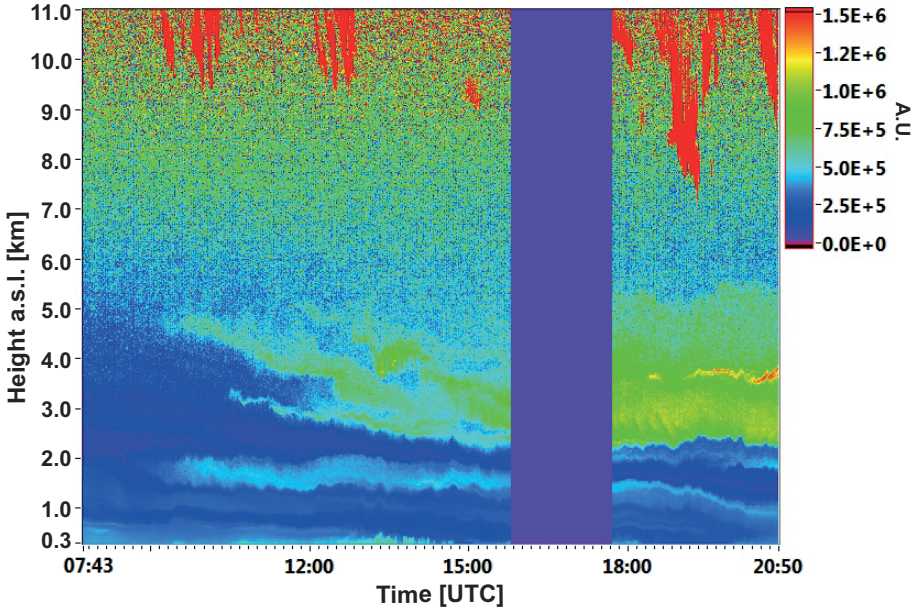

Figure 3. Saharan dust outbreak advecting dust particles between 2 and 6 km height towards Limassol, Cyprus, on 23 May 2013. Range-corrected 1064 nm backscatter signals (in arbitrary units, A. U.) are shown.

ACPD
15, 5203–5240, 2015

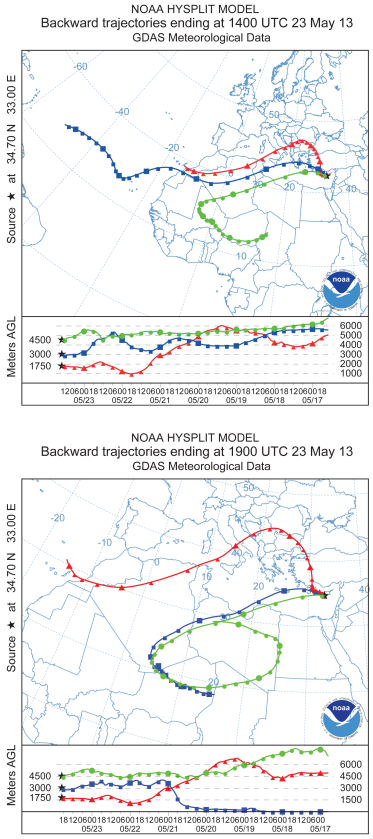

Figure 4. Seven-day HYSPLIT backward trajectories arriving at Limassol, Cyprus, at 1750 m (red), 3000 m (blue), and 4500 m height (green) on 23 May 2013, 14:00 UTC (top) and 19:00 UTC (bottom).

ACPD
15, 5203–5240, 2015

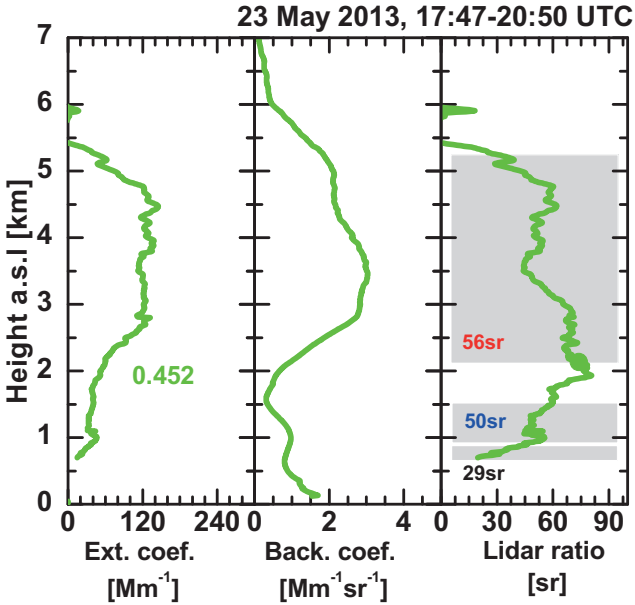

Figure 5. Mean vertical profiles of the 532 nm particle extinction coefficient, backscatter coefficient, and lidar ratio for the observational period from 17:47–20:50 UTC on 23 May 2013. The Raman lidar method is applied. Vertical signal smoothing lengths of 600 m (below 1.1 km height), 1500 m (1.1–2.8 km height), and 2100 m (above 2.8 km height) are applied before computing the extinction coefficients and lidar ratios. The signal smoothing length is 750 m for the shown backscatter coefficient profile. Total AOT (given as number in the left panel) and layer mean values of the lidar ratio for the 0.7–0.85 km height layer (influenced by marine and local pollution particles), the 0.86–1.5 km layer (influenced by aged European haze) and for the pure dust layer (2.1–5.2 km height range) are given as numbers. Retrieval uncertainties are of the order of 10 % (backscatter coefficient), 25 % (extinction coefficient), and 30 % (lidar ratio).

ACPD
15, 5203–5240, 2015

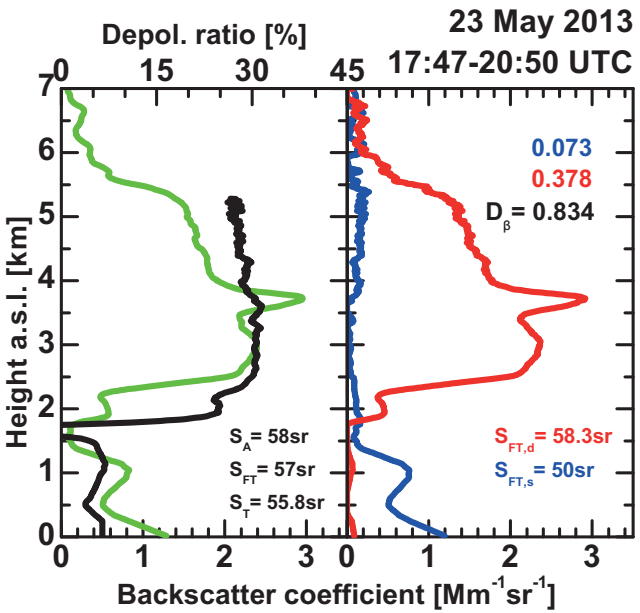

Figure 6. Mean profiles (3 h average) of the 532 nm particle backscatter coefficient (left, green), particle linear depolarization ratio (left, black), dust backscatter coefficient (right, red), and non-dust particle backscatter coefficient (right, blue). The elastic-backscatter lidar method (explained in Sect. 3) is applied to the same observation as shown in Fig. 5. Retrieved column lidar ratios for the total troposphere (S_T), the free troposphere (S_{FT}), and derived from the AERONET data (S_A for the 13:00–14:00 UTC period) for the total tropospheric column after Schuster et al. (2012) are given as numbers in the left panel. S_{PBL} of 30 sr is assumed for the height range up to 500 m. The retrieved dust-related lidar ratio $S_{FT,d}$ and the assumed non-dust lidar ratio ($S_{FT,s}$) are given in the right panel together with the dust AOT (red number), non-dust AOT (blue number) for the total troposphere, and the FT dust backscatter fractions D_β (column dust backscatter to total particle backscatter in the free troposphere above 500 m height).

ACPD
15, 5203–5240, 2015

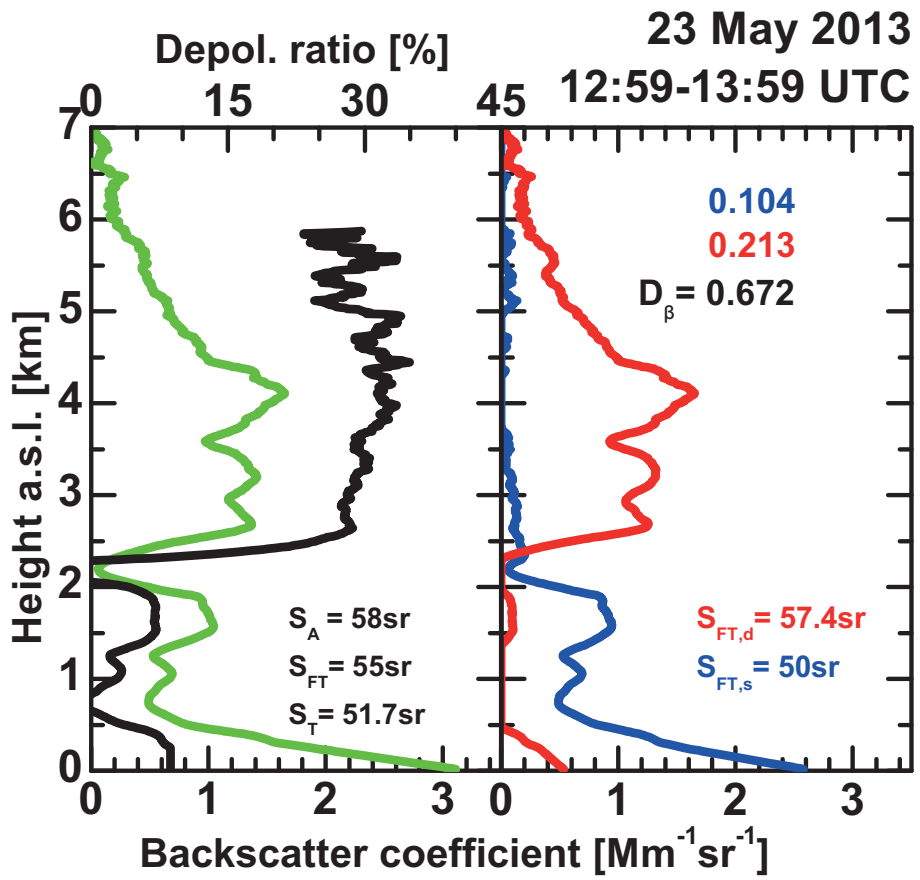

Figure 7. Same as Fig. 6, except for 23 May 2013, 12:59–13:59 UTC.

ACPD
15, 5203–5240, 2015

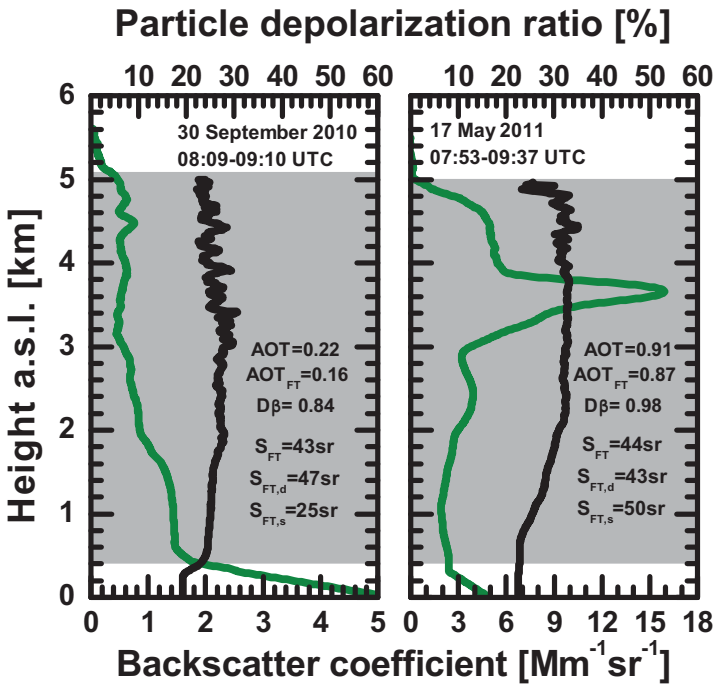

Figure 8. 532 nm particle backscatter coefficient (green) and particle linear depolarization ratio (black) during a Saharan dust outbreak on 30 September 2010 (left) and a Middle East desert dust outbreak on 17 May 2011 (right). The gray-shaded areas indicate the identified main FT dust layers. Total tropospheric AOT, AOT_{FT} for the free troposphere, and several retrieved lidar ratios (S_{FT}, $S_{FT,d}$) are given as numbers. Assumed lidar ratios are S_{PBL} = 30 sr and $S_{FT,s}$ = 25 sr (left panel) and 50 sr (right panel).

ACPD
15, 5203–5240, 2015

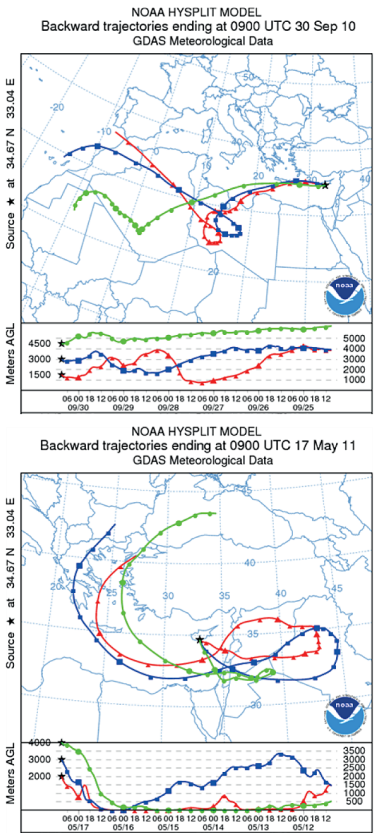

Figure 9. Six-day HYSPLIT backward trajectories arriving at Limassol, Cyprus, at 1500 m (red, top) and 2000 m (red, bottom), 3000 m (blue), 4000 m (green, bottom), and 4500 m height (green, top) on 30 September 2010, 09:00 UTC (top) and 17 May 2011, 09:00 UTC (bottom).

ACPD
15, 5203–5240, 2015

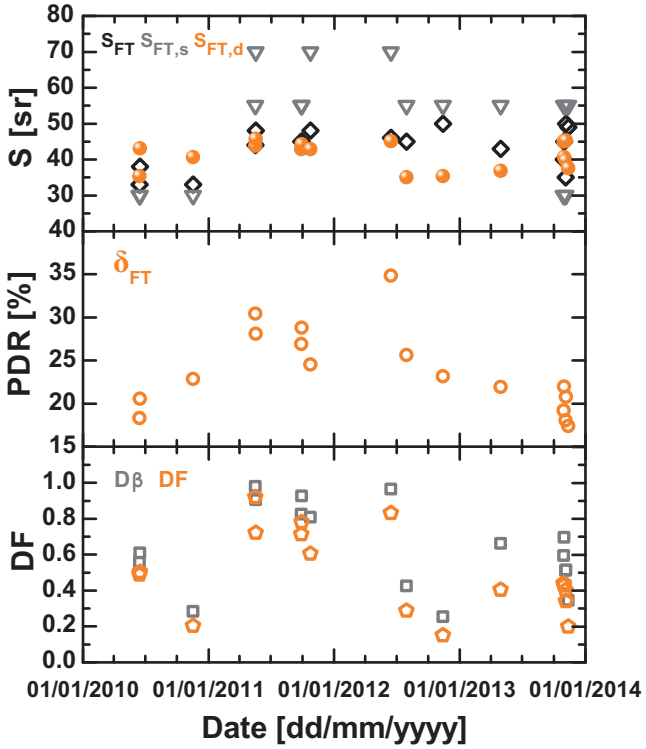

Figure 10. (Top) Retrieved FT 532 nm lidar ratio S_{FT} (black diamonds), dust-related lidar ratio $S_{FT,d}$ (orange circles), and assumed non-dust lidar ratio $S_{FT,s}$ (gray triangles) for 17 Middle East dust outbreaks, (center) mean 532 nm particle linear depolarization ratio δ_{FT} for the entire free troposphere (above the PBL), and (bottom) 532 nm AOT dust fraction DF (orange pentagons, dust AOT to total AOT), and FT dust backscatter fraction D_β (gray squares).

ACPD
15, 5203–5240, 2015

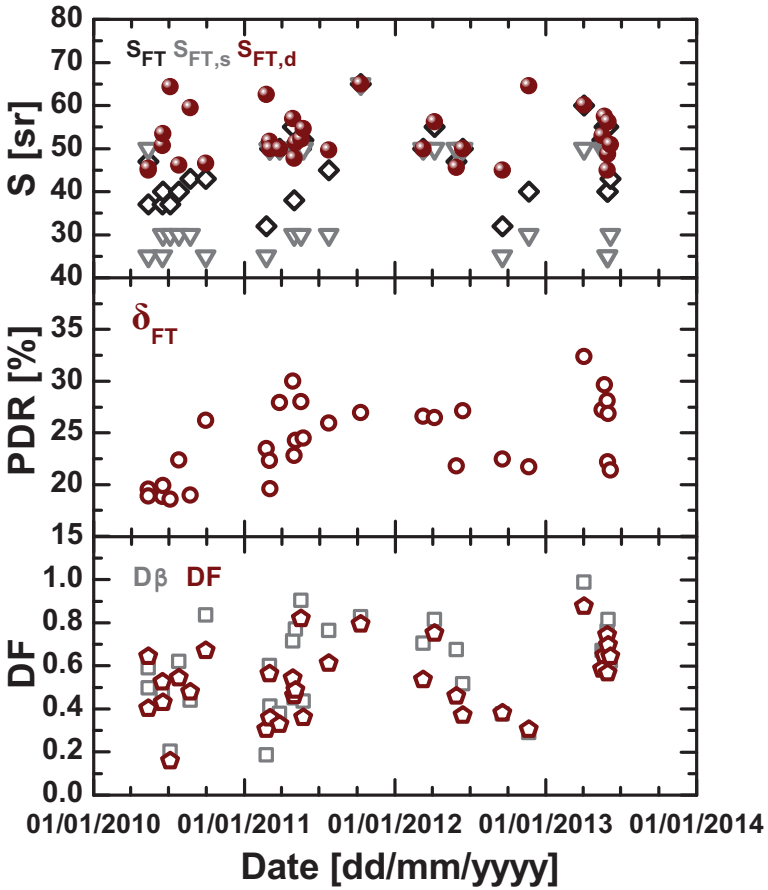

Figure 11. Same as Fig. 10, except for Saharan dust outbreaks.

ACPD
15, 5203–5240, 2015

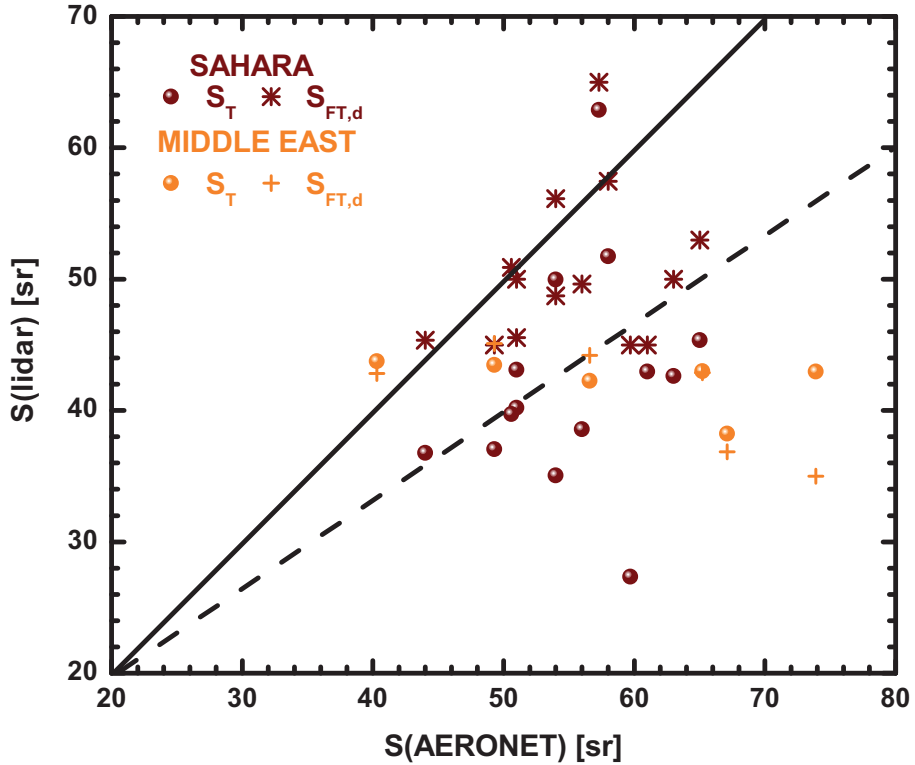

Figure 12. Lidar-derived total tropospheric lidar ratio S_T vs. respective AERONET-derived lidar ratio S_A after Schuster et al. (2012). The solid and dashed lines shows the 1 : 1 and the 1 : 1.2 correlation lines, respectively. The AERONET S_A values are in most cases larger than the lidar-derived S_T values (and thus below the 1 : 1 line). For comparison the dust-related lidar ratios $S_{FT,d}$ (from the lidar retrieval) are also shown (stars, crosses).

ACPD
15, 5203–5240, 2015